

RLFC: Random Access Light Field Compression using Key Views

Srihari Pratapa

Department of Computer Science
UNC Chapel Hill
psrihariv@cs.unc.edu

Dinesh Manocha

Department of Computer Science
UMD, College Park
dm@cs.umd.edu

ABSTRACT

We present a new hierarchical based compression scheme for encoding light field images (LFI) suitable for interactive rendering. Our method (RLFC) exploits redundancies in the light field representation by constructing a hierarchical tree structure. The top level (root) of the tree captures the common high-level details across the LFI, and other levels (children) of the tree capture specific low-level details of LFI. Our decompressing algorithm corresponds to a tree traversal operation, which gathers the values stored at different levels of the tree. Our approach provides random access with one level of indirection, parallel decoding, and enables fast interactive rendering. We have implemented our method for 4D two plane parameterized light fields. The compression rates vary from 0.1 – 3 bits per pixel (bpp), resulting in compression ratios of around 200:1 to 10:1 for PSNR quality of 35 to 50 dB. As compared to prior random access schemes, we observe 5 – 10X improvement in compression rate for similar PSNR quality. The decompression times for decoding the required blocks of LFI are approximately 2 – 5 microseconds. Our overall scheme is simple to implement and involves memory operations, bit manipulations, and arithmetic operations.

ACM Reference Format:

Srihari Pratapa and Dinesh Manocha. 2017. RLFC: Random Access Light Field Compression using Key Views. In *Proceedings of Conference Name*. ACM, New York, NY, USA, 9 pages. <https://doi.org/10.1145/8888888.7777777>

1 INTRODUCTION

Light fields create a photo-realistic rendering of extremely complex scenes that are difficult to achieve with other conventional rendering techniques. The photo-realistic rendering from light fields makes Virtual Reality (VR) content more immersive and improves presence in realistic scenes. Levoy and Hanrahan 1996 and Gortler et al. 1996 described LF rendering methods by capturing a scene using a grid of camera array for a scene. This has been an active area of research for more than two decades. Many improved methods for capturing and rendering light fields have been proposed. Several hand held plenoptic cameras have been developed to capture high stereo light fields of real scenes [Ng et al. 2005; Perwass and Wietzke 2012] and use them for VR applications [Yu 2017].

One of the primary bottlenecks of image-based rendering (IBR) approaches is the amount of data needed to capture the 3D scenes

using image samples. IBR techniques generate a lot of images to sample the light rays of a given scene. Typically, uncompressed light field images sizes can vary from 200MB to 10GB (or more) and can be even larger depending on the sampling rate and image resolution. Several methods and hardware techniques for interactive rendering of light fields have been proposed [Chen et al. 2002; Jones et al. 2007]. The need for using high resolution light fields has increased with recent demand for high resolution multimedia content (2K or 4K resolution). An efficient way to capture high resolution panoramic light field is discussed in Birkblauer et al. [2013].

In order to store, transmit and render LFI, it is important to develop good compression algorithms. Different schemes have been put forward for compressing LFI, as surveyed in [Viola et al. 2017]. The majority of the methods provide high compression rates, similar to standard 2D image compression methods, but they require decoding of all the LFI samples into memory before rendering. During rendering, any of the sampled light rays (pixels) from the LFI may be used for computing new views. For interactive rendering, it is necessary that the compressed LFI bitstream has random access property. Random access to the compressed LFI bitstream can reduce the memory footprint of rendering by a significant factor. Some prior random-access compression schemes based on vector-quantization or wavelets have been proposed [Levoy and Hanrahan 1996; Peter and Straßer 2001], but they may not be able to provide high compression rates or make some assumptions about the scenes.

Main Results: We present a new hierarchical compression scheme (RLFC) for encoding high-resolution light field images for interactive rendering. Our method is based on clustering spatially close sampled images of light fields and constructing levels of a tree. The root of the tree stores the common features or characteristics among the LFI; the rest of the children nodes of the tree store the specific low-level or sparse details of the LFI. In our hierarchical tree construction, the images that capture the high-level common details among the LFI are referred to as *representative key views (RKV)* and low-level specific detail images are referred to as *sparse residual views (SRV)*. We construct the tree recursively until we compute the desired number of levels, starting with the original LFI at the bottom level RKV. Once the tree is built, the top level of the tree contains RKV images similar to original LFI and are compressed using standard image compression methods (e.g., JPEG2000). The children nodes contain SRV, which correspond to highly sparse images and are easy to compress. At all levels, the SRV are divided into blocks and only the blocks with significant details are stored. The significant blocks of the residual images are encoded using Bounded Sequence Integer Encoding [Nystad et al. 2012]. The resulting compressed bitstream is represented to support selective decoding and provide random access to blocks of pixels with only one level of indirection. Retrieving a pixel value is a tree traversal

Permission to make digital or hard copies of all or part of this work for personal or classroom use is granted without fee provided that copies are not made or distributed for profit or commercial advantage and that copies bear this notice and the full citation on the first page. Copyrights for components of this work owned by others than ACM must be honored. Abstracting with credit is permitted. To copy otherwise, or republish, to post on servers or to redistribute to lists, requires prior specific permission and/or a fee. Request permissions from permissions@acm.org.

Conference Name, Conference Date and Year, Conference Location

© 2017 Association for Computing Machinery.

ACM ISBN 978-1-4503-1234-5/17/07...\$15.00

<https://doi.org/10.1145/8888888.7777777>

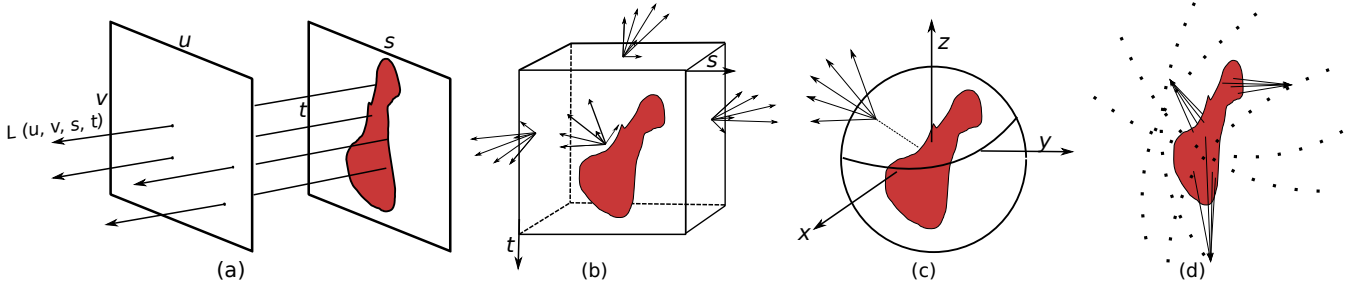


Figure 1: (a) 4D parametrization of the plenoptic function, the light field. In this representation, all the light rays coming out of (u, v) focused on the (s, t) are sampled. (b) The lumigraph, in which a bounding cube is used to bound the interesting region. (c) In the spherical parameterization, the region of interest or object is bounded in a sphere, and the light rays coming out of the surface are sampled. (d) The unstructured light field, in which the light rays are densely sampled without any strict fixed structure, all around the object at different points in space. Our approach is applicable to all these parameterizations.

operation that gathers SRV blocks and combines them with the RKV blocks at the top-level. We have implemented our method on the 4D two plane parameterization of light fields and present the results on the Stanford light field archive. The decoding times to compress a block of pixels from our compressed stream are approximately 2-5 milliseconds.

We obtain compression ratios of around 200 : 1 to 10 : 1 for PSNR quality of 35 – 45 dB. As compared to prior random-access LFI compression schemes, we observe 5 – 10X improvement in compression rates for the same quality. Furthermore, we make no assumptions about the scene and our approach can be applied to other light field parameterizations.

The remainder of the paper is organized as follows: Section 2 gives an overview of prior work in image based rendering, light fields, and light field compression. Section 3 gives the details about compression, decompression, and the benefits of our approach. In Section 4, we present detailed analysis of our compression scheme. Limitations and future work are discussed in Section 5.

2 BACKGROUND

In this section, we present a brief overview of Light fields, image-based rendering, and light field compression methods.

2.1 Image-Based Rendering

Adelson et al. [1991] used the term *plenoptic function* to describe the light intensity (L) at any point (x, y, z) ; orientation (θ, ϕ) in free space; at any given time (t); and over a range wavelengths (λ) in the visible spectrum: $L = P(x, y, z, \theta, \phi, t, \lambda)$. The plenoptic function describes the flow of light in space. Measuring the plenoptic function, a 7-dimensional (7D) function would allow a true holographic reconstruction of the real world around us.

Over the last few decades several image-based rendering techniques using a low dimensional form of the 7D plenoptic function have been described [Beier and Neely 1992; Chen and Williams 1993; Lippman 1980; McMillan and Bishop 1995]. Intensity of light rays through empty space remains constant, Levoy and Hanrahan [1996] used this observation to present a simple two plane (4D) parametrization of the plenoptic function. In this two plane parameterization, all the light rays between parallel planes are described using a pair of parameters (u, v) and (s, t) . The light rays between the

two planes were called *light slab* and the 4D parametrized plenoptic function was named *light field* (LF). In Gortler et al. [1996] a 4D parametrization similar to light field, called *lumigraph* was introduced. In lumigraph, instead of two parallel planes a cube is used to bound a particular region of interest in space. Due to its elegance and simplicity, the two plane light field parameterization is widely adapted in practical applications [Ng et al. 2005; Perwass and Wietzke 2012; Yu 2017]. In Ihm et al. [1997], the light rays coming out of the spheres surface are sampled. Following lumigraph, a spherical parametrization [Ihm et al. 1997] of the light field is one in which the object of interest is surround by a sphere instead of a cube. In all the above parameterizations the light rays are captured as discrete samples using camera images. The above parameterizations have an inherent uniform structure associated with sampling the light rays in the region of interest. Extending further, the idea of unstructured light fields [Davis et al. 2012] and unstructured lumigraph [Buehler et al. 2001] was introduced in which no strict order is imposed on the sampling of the light rays of the region of interest. Using the method described in Davis et al. [2012], any scene can be captured with a hand-held camera and rendered back.

2.2 Light Field Compression

The minimum sampling rate required for a good reconstruction using IBR is a well studied problem [Chai et al. 2000; Chan and Shum 2000; Lin and Shum 2000]. Even with a minimal sampling rate, the number of image samples required is of the order of thousands for a good quality reconstruction [Chai et al. 2000]. Many schemes have been proposed for LFI compression and we categorize the existing compression schemes into two categories; *high efficiency encoding schemes*, which include methods similar to standard image and video coding techniques (DCT, wavelet), and *random access compression schemes*, which include methods suitable for fast IBR and viewing as they provide fast random access to specific pixels. In response to the growing interest in quality plenoptic VR content the JPEG standardization committee launched JPEG Pleno [Ebrahimi et al. 2016]. The aim of the JPEG Pleno is to find and define standards for wide adaptability of 4D LF compression similar to JPEG and MPEG standards.

2.2.1 High efficiency LFI compression schemes: Initial work on IBR compression is based on extending the standard image and

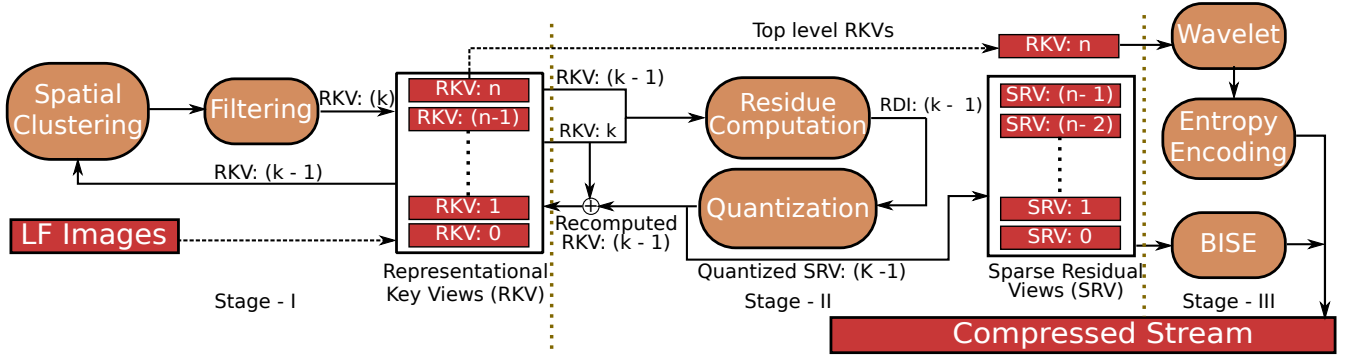


Figure 2: The red rectangles represent data, brown oval rectangles represent processing blocks, arrows indicate flow and data transfer operations. Our compression pipeline: The compression pipeline comprises of three stages. (Stage - I) The first stage is computing hierarchical representational key views (RKV), where each level is computed by filtering clusters from the previous level. (Stage- II) The second stage consists of computing sparse residual views (SRV) top down approach starting at top level. (Stage - III) In the third stage, the top level RKV and SRV levels are further processed to compute the compressed bitstream.

video coding methods to LF images, with proper modifications or extensions. These methods employ techniques such as discrete-cosine transform, wavelet transform, predictive block encoding, and motion-vector compensation used in standard methods (JPEG, JPEG200, MPEG-2, MPEG-4). Disparity compensation instead of motion vectors for predictive coding blocks of LF Images is used in Girod et al. [2003]; Jagmohan et al. [2003]; Magnor and Girod [2000]. In the disparity compensated approaches, a pre-fixed set of LF images are encoded independently (I-frames) and the rest of the LF image blocks are encoded predictively (P-frames) from I-frame blocks. Due to the uniform camera motion in 4D parameterization (Fig.1(a)), P-frame blocks can be predicted from I-frame blocks using a single disparity value. The compression rates of these methods are around 100:1 to 200:1, depending on the details in the original LFI. Kundu [2012] uses homography techniques to predictively encode LF images (P-frames) by warping them onto a set of I-frames, achieving compression rates of 10:1 to 50:1. Chang et al. [2003, 2006] introduced, methods based on using additional shape and geometry information of the object captured in the LF images. More recently, methods directly based on HEVC video coding are proposed in Chen et al. [2018]; Liu et al. [2016]; Perra and Assuncao [2016] for high compression rates of 100:1 to 1000:1. In 2016 the LF-Images are ordered using a pseudo-sequence temporal ordering and compressed using HEVC encoding. Chen et al. [2018] used a small set of key-views to predict the rest of the images using disparity based image-transformations, followed by the pseudo-sequence method in Liu et al. [2016]. Methods in Chen et al. [2018]; Liu et al. [2016] are designed specifically for Lytro cameras, which capture images at 10 bits per pixel precision.

2.2.2 Random Access LFI compression: Levoy et al. 1996 presented a compression technique using vector-quantization (VQ) that provides random access for interactive rendering. VQ provides compression rates of around 10:1 to 20:1 but the compression quality is low. However, VQ based compression fails to take advantage of the high correlations present among LF images. Peter et al. 2001 described an approach for random access compression using a 4D wavelet hierarchical scheme providing compression rates of 20:1 to 40:1. However, the method requires multi-level caches for fast

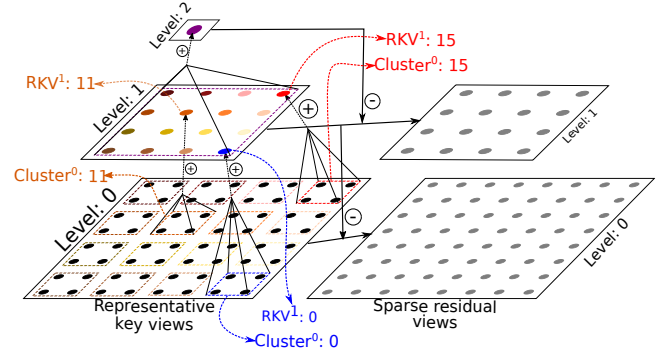


Figure 3: We highlight the construction of hierarchical representational key views (RKV) and sparse residual views (SRV) for 4D two plane LF parametrization. Level:0 has the original LF image samples. Level:1 is constructed by filtering clusters of four spatially close images. Level: 2 is constructed by filtering all the images on level: 1. Sparse residual views (SRV) are constructed in a top down manner by computing the differences between alternative levels of representational views.

data access while rendering. The method also makes assumptions on the scene captured in the light fields. The goal of our method is to provide compression rates closer to the *high efficiency encoding* discussed above and have random access. We also make sure that our method is hardware friendly by limiting the compression decomposition to simple bit manipulation and arithmetic operations.

3 OUR METHOD

In this section, we present the details of our encoding approach and an overview of our compression pipeline (Figure 2). The input to our method is LFI samples of a scene and the output is a compressed stream that is random access decodable with one level of indirection. Our method is designed to work with any of the LF parameterizations shown in Figure 1. Our approach has the following components:

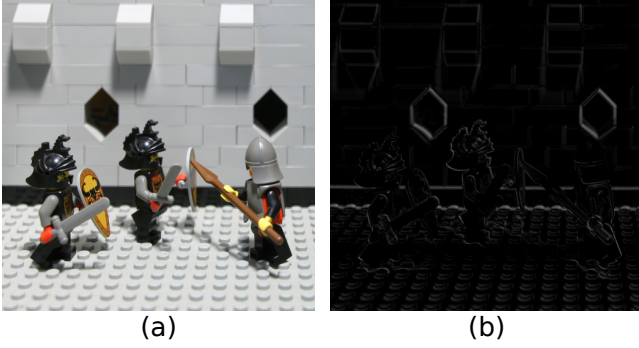


Figure 4: Example (a) representative key view and (b) sparse residual view image. We can see that the residual view image is highly sparse with large intensity pixel values constrained in small regions. The images belongs to Lego Knights LF from the Stanford light field archive

- **Representative Key Views (RKV):** At each level of the tree, these images capture the common details present in the images in the level below it.
- **Sparse Residual Views (SRV):** At each level of the tree, these images capture the specific details of the images in the current level.
- **Clusters (C):** At each level of the tree we cluster spatially close by samples of RKV and compute the RKV of the next level of the tree.

We construct a hierarchical tree with the root node storing representative key views (RKV) and the children nodes storing the sparse residual views (SRV). We start by setting the input indexed LFI samples as the bottom level (zero level) of the tree and recursively construct higher level RKV of the tree starting at the bottom. At any given level, we cluster the spatially close by RKV images; for each cluster we compute the RKV of the next level of the tree. Once the RKV tree is computed, we compute the SRV for each level from top to bottom, reconstructing RKV images after a quantization of SRV at each level of the tree. Next, we encode the RKV images at the top level (root) of the tree using standard image compression techniques such as JPEG200. Each level of SRV is divided into blocks and compressed using bounded integer sequence encoding (BISE) [Nystad et al. 2012]. The rest of the section describes the steps involved in the construction of the tree in detail. Further, we discuss the arrangement of the BISE compressed RDI blocks in the final compressed stream to enable selective decompression with random access.

Notation: We use the following short forms and notation while presenting our approach: *Representational key views*: RKV; *Sparse residual views*: SRV; *Bounded Integer Sequence Encoding*: BISE; **RKV** denotes the representative key view tree; **RKV^l** denotes the set of all representational key views at level l of the tree; $(RKV_i)^l$ denotes the i^{th} representational key view at level l ; SRV denotes the sparse residual view tree; **SRV^l** denotes the set of all sparse residual views at level l of the tree; $(SRV_i)^l$ denotes the i^{th} sparse residual view at level l ; $(C_j)^l$ denotes the j^{th} set of clustered RKV samples on the level l .

Algorithm 1 Compress light field image samples

Input:

Original indexed light field images: **LFI**

Encoding parameters: *enc*

Output:

Compressed stream

function COMPRESSLFI(LFI, *enc*)

//Set the bottom level of RKV tree to LFI samples

RKV⁰ \leftarrow LFI

RKV \leftarrow ComputeRKVTree(RKV⁰, *enc*)

SRV \leftarrow ComputeSRVTree(RKV, *enc*)

//Compress top level RKVⁿ using JPEG2000

RKVStream \leftarrow JPEG2000(RKVⁿ)

//Initialize the SRV tree compressed bitstream to empty

SRVStream \leftarrow 0

BlockOffsets \leftarrow {}

//Process all the blocks

for each index *in* blocks **do**

/*Travel the SRV tree in a level order fashion to gather the blocks*/

OrderedBlocks \leftarrow LevelOrder(SRV, index)

//Encode the blocks of SRV levels using BISE

OrderedBlocksBISE \leftarrow BISEEncode(LvlBlocks)

BlockOffsets \leftarrow Sizeof(OrderedBlocksBISE)

SRVStream \leftarrow SRVStream: OrderedBlockBISE

//Append the streams and return the final stream

return (RKVStream: BlockOffsets: SRVStream)

3.1 Representational Key Views

In the different parameterizations discussed in Section 2.1, the light fields are sampled at different spatial locations. The image samples exhibit strong spatial correlations and we exploit these correlations to find redundancies and compress the data. The first step is to cluster spatially close by samples using the number of clusters and number of images in each cluster set as an encoding parameter for all the levels.

$$C_j^{(l-1)} = \bigcup RKV_m^{(l-1)} \quad (1)$$

$$m \in \{k_1, k_2, \dots, k_n \mid \text{dist}(k_u, k_v) < \text{threshold}\}$$

For each cluster of image samples, an RKV image is computed. The RKV image is computed using a weighted filtering of all the images in the cluster. Let $(C_j)^{(l-1)}$ be the j^{th} cluster on level $(l-1)$, I denote an RKV in the current cluster and the $(RKV_j)^l$ on level l is computed as:

$$RKV_j^l = \int_{C_j^{(l-1)}} w_j^{(l-1)}(I) * C_j^{(l-1)}(I) dI \quad (2)$$

$w_j^{(l-1)}(I)$ indicates the weight function for filtering images in the cluster $C_j^{(l-1)}$. The new set of **RKV^l** images computed at a level (l) exhibit spatial correlations similar to the **RKV^(l-1)** images at the level below $(l-1)$. This process is recursively repeated until a certain number of levels of the tree are computed, which is set as an encoding parameter. This generates hierarchical levels of RKV

creating a child-parent relationship between the cluster of images $C_j^{(l-1)}$ on level $(l-1)$ and the corresponding RV_j^l image on level l , computed from the cluster. Figure 3 illustrates this process for a given 4D two plane parameterization.

3.2 Sparse Residual Views

Once the RKV tree is constructed, the SRV tree is computed in a top down fashion, starting with the top-level of the RKV tree. The $SRV^{(l-1)}$ at level $(l-1)$ are computed by subtracting the parent $(RKVP)^l$ on level l from the corresponding children RKV^{l-1} on level $l-1$. The $SRV_i^{(l-1)}$ on level $(l-1)$ is computed as:

$$(SRV_i)^{(l-1)} = (RKV_i)^{(l-1)} - (RKVP)^l \quad (3)$$

The SKV images are quite sparse and consists of small concentrated regions of high intensity values. Figure 4 shows example RKV and SRV computed using our approach. It can be seen that SRV image is mostly empty with zero or small intensity with only certain regions of high intensity pixels. Based on this observation, we divide all the levels of SRV images into non-overlapping rectangular blocks and only store blocks with high intensity pixel values. We process the SKV images with two levels of quantizations; pixel value quantization and block energy quantization based on thresholds set as encoding parameters. The pixel threshold values determine whether a pixel in an SRV image provides sufficient contribution, otherwise it is set to zero. The block energy based quantization computes the sum of the absolute pixel values in a block and decides if a block is significant. Once the $SRV^{(l-1)}$ at level $(l-1)$ is computed, the corresponding $RKV^{(l-1)}$ of the level are recomputed. We recompute $RKV^{(l-1)}$ so that the quantization errors do not propagate down the tree to the levels below. At the end of the downward pass we are left with a set of top level (n) RKV^n and an SRV tree. The RKV^n at the root of the tree are compressed using standard image compression techniques (JPEG, JPEG2000). The blocks of SKV images on all levels of the tree are compressed using Bounded integer sequence encoding [Nystad et al. 2012].

3.3 Compressed Stream Structure

We arrange the final compressed stream to enable progressive decoding and random access with one level of indirection to decode the required pixels. For each block, we perform a level order travel on the SRV tree from the top and gather all the BISE encoded blocks level-wise. The BISE bitstreams of significant blocks are appended to the final stream. To identify the significant blocks, we need to store a binary map to indicate if a block is significant. To decompress a BISE encode stream, the maximum value in the stream is required. Instead of an additional significance map, we store an array of maximum values, and a zero value indicates a non-significant block. An array of block offset values to the start location of each block in the final stream is stored to facilitate parallel decompression. Figure 5 visually depicts the compressed structure described.

3.4 Decompression & Random access

The first step in decompression is decoding all the top level RKV images. To decode a block of pixels at a particular location we traverse the SRV tree and, gather the BISE streams of all the corresponding

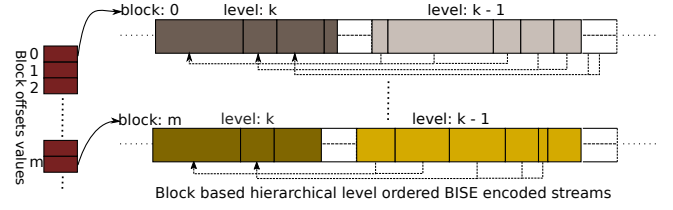


Figure 5: The arrangement of the SRV tree in the final compressed stream. For each block in the SRV tree we store the significant block BISE streams in a level order fashion starting from the top. For each block the start locations of the level ordered BISE streams in a block offset array.

Algorithm 2 Decompress light field image block

Input:

LFI compressed stream: **CompLFI**
 Image index: **ImgIdx**
 Block index: **BlkIdx**

Output:

Pixel values: **PixVals**
 // Load the stream into memory and separate into parts

Initialization:

$RKVStream \leftarrow ReadRKVStream(CompLFI)$
 $RKV^n \leftarrow DecompressJPEG2000(RKVStream)$
 $BlockOffsets \leftarrow ReadBlockOffsets(CompLFI)$
 $SRVStream \leftarrow ReadSRVStream(CompLFI)$

function DECOMPRESSLFI_BLOCK(ImgIdx, BlkIdx)

// Get the start location of BlkIdx in bitstream
 $StartOffset \leftarrow BlockOffsets[BlkIdx]$
 // Read the top level filtered values from RKV
 $RKVBlock \leftarrow ReadBlock(RKV^n, BlkIdx)$
 // Compute the location of the parent blocks in stream
 $ParentIdx \leftarrow GetParentIndices(ImgIdx)$
 // Read the BISE encoded stream of required blocks
 $OrderedBlockBISE \leftarrow ReadBlocks(SRVStream, ParentIdx)$
 // Decode the BISE blocks
 $OrderedBlocks \leftarrow BISEDecode(OrderedBlockBISE)$
 // Combine the residual values with filtered pixel values
 $PixVals \leftarrow CombineBlocks(RKVBlock, OrderedBlocks)$

blocks until it reaches the bottom level. Next, the residual pixel values are gathered by decoding the BISE streams. Finally, the pixel values of are computed by combining the residual pixel values with the corresponding top level RKV image. In the tree traversal operation, we selectively gather and decode only the required blocks. With selective decoding, the compressed data stays compressed in the memory, except for the required parts.

Given a pixel's location, we can compute block location and the location of all parent blocks in a compressed stream using the level order arrangement. The start location of the current block's compressed stream is located using the block offset values. Using the selective tree traversal decompression, our approach provides random access to the pixel values at block level without decompressing the other parts of the compressed data.

3.5 Interactive Rendering

Our decompression scheme is designed to be compatible with several efficient IBR techniques [Isaksen et al. 2000; Levoy and Hanrahan 1996] by supporting block based parallel and progressive decompression. It is evident from the arrangement of compressed stream as shown Figure 5, our method supports parallel decoding of multiple blocks at once. Our method inherently supports progressive decompression as the *RKV* tree built during the compression has filtered images of spatially close by LF images at different levels. For progressive decompression we can modify the tree travel operation to stop and compute the high-level filtered pixel value at a certain level. The rendering scheme can be progressively updated the pixel values as decompressor computes the final pixel values in the background. Parallel and progressive decompression supported by our method makes improves the rendering rate by a significant factor. The decompression scheme is also hardware friendly as the decoding operations are limited to just memory reading and simple integer arithmetic operations. Bounded integer sequence encoding (BISE) is hardware decompressible as pointed in Nystad et al. [2012].

3.6 Performance Analysis

Algorithm 1 gives a high level pseudo-code of our compression scheme. The primary operations involved in our compressing scheme are: (1) Filtering of images; (2) Compressing top level of *RKV* tree; (3) Rearranging blocks of memory, *SRV* Tree level order traversal; (4) BISE encoding of sparse residual blocks.

Algorithm 2 highlights the steps in the decompression scheme. At the start of the rendering operation, the final compressed stream is loaded into the memory and top level *RKV* images are decompressed. The operations used in the block computation include: (1) loading required bytes from in memory *SRV*Stream into registers; (2) bit manipulation operations required for decoding BISE compressed blocks; (3) simple arithmetic operations to combine the *SRV* pixel values with *RKV* pixel values;. Our decompression scheme is hardware friendly as the operations include memory reads, bit manipulation, and simple integer arithmetic.

4 RESULTS

We have implemented RLFC for the 4D two plane parameterized LF. We have tested and analyzed our approach on the Stanford light field archives [Levoy and Hanrahan 1996; Wilburn et al. 2005]. The LFI in the dataset Wilburn et al. [2005] are high resolution images captured using large camera arrays. The input LF images are 24-bit depth RGB images. we use lossless YCoCg-R [Malvar et al. 2008] color space to decorrelate the color channels. During all stages of our compression scheme, we use lossless integer computations adjusting the required dynamic range. We measure the compression rate using bits per pixel (bpp). In the current implementation, we compress the top level representative views using the JPEG2000 lossless algorithm. The quality is measured using *peak-signal-to-noise-ratio*($PSNR_{YCoCg}$) as the weighted average [Ohm et al. 2012] of the PSNR individual components:

$$PSNR_{YCoCg} = \frac{6 * PSNR_Y + PSNR_{Co} + PSNR_{Cg}}{8} \quad (4)$$

LF Dataset (Resolution): Size (MB)	Compression rate (bpp)	PSNR (dB)
Dragon ($32 \times 32 \times 256 \times 256$) : 192	0.420	41.39
Budhha ($32 \times 32 \times 256 \times 256$) : 192	0.097	41.21
Amethyst ($16 \times 16 \times 768 \times 1024$) : 576	0.198	41.99
Bracelet ($16 \times 16 \times 1024 \times 640$) : 480	0.805	42.31
Bunny ($16 \times 16 \times 1024 \times 1024$) : 768	0.130	41.05
Jelly Beans ($16 \times 16 \times 1024 \times 512$) : 384	0.186	41.10
Lego Knights ($16 \times 16 \times 1024 \times 1024$) : 768	1.20	40.64
Lego Gallantry ($16 \times 16 \times 640 \times 1024$) : 480	1.12	40.15
Tarot Cards ($16 \times 16 \times 1024 \times 1024$) : 768	2.29	41.99

Table 1: The compression rates and quality for several LF datasets from Stanford light field archive. All the image samples are 24-bit depth RGB images. For a similar PSNR quality the compression rate varies differently for each LF depending on the details of the scene recorded in the LF.

The PSNR of each component is measured as:

$$PSNR = 10 * \log_{10} \frac{255^2}{MSE} \quad (5)$$

Where MSE is the mean square error between the original images and decompressed images in the LF. The final PSNR is computed as the average overall the images in LF samples.

Table 1 shows the compression rate and PSNR for several LF Datasets for a *block size*: 2; *tree height*: 3. The *block threshold* is adjusted for each dataset to achieve a similar decompression quality. The compression rate varies from 0.1 – 2.3 bpp for a similar PSNR quality depending on the details of scene captured in the LF. Our method provides 5 – 10× better compression compared to previous methods that provide random access [Peter and Straßer 2001] for similar PSNR quality.

Our method has several encoding parameters, with primary parameters being *tree height* (number of levels in the hierarchy), *block size*, *block threshold* (threshold on the sparse residual blocks). We measure the effect of encoding parameters on the resulting compression rate, and quality. Table 2 highlights the effect of changing the *block size* on the bpp and PSNR with *block threshold* and *tree height* set as constants. For a fixed *block threshold*, increasing *block size* increases the energy (absolute sum of pixel values) of the residual blocks reducing the quantization errors, resulting in higher bpp and PSNR. In Table 3, we change the *tree height* to see variations in the resulting bpp and PSNR. We notice that with increase in the *tree height*, the sparsity of the residual views in each level increases. With a fixed *block threshold*, the quantization errors are increased with increase in sparsity and a slight reduction in the bpp and quality is observed.

In Figure 7 and Figure 8 the outcome of varying the *block threshold* on the bpp and PSNR are shown respectively. Increase in the *block threshold* implies increase in the quantization errors of the sparse residual blocks resulting in the decrease of bpp and PSNR. Variation of increase in the resulting quality with increase in the bpp is shown in Figure 9. The variation of the decompression quality with bpp is subjective to the details in the LF under consideration. Figure 6 shows zoomed in visual quality comparison of interesting regions of few images from LF Dataset. The comparison shows that our compression method introduces no visible artifacts in the LF images.

LF Dataset	Metric	Block Size: 2	Block Size: 4	Block Size: 8
Amethyst	bpp	0.155	0.508	1.33
	PSNR	40.82	46.69	51.91
Bunny	bpp	0.130	0.438	1.45
	PSNR	41.04	46.31	52.18
Bracelet	bpp	0.73	1.16	1.84
	PSNR	40.51	48.45	52.85
Knight	bpp	0.60	1.26	2.15
	PSNR	38.96	47.45	53.51

Table 2: We highlight the variation in the resulting compression rate and quality, as the block size changes. we set the block threshold to 50 and the tree height to 3, for all the datasets. For a fixed block threshold, the quantization errors decrease when the block size increases. As a result, we observe an increase in bpp and PSNR.

LF Dataset	Metric	Tree Height: 3	Tree Height: 4	Tree Height: 5
Amethyst	bpp	0.407	0.357	0.352
	PSNR	45.28	44.74	44.45
Bunny	bpp	0.34	0.276	0.265
	PSNR	45.15	44.70	44.35
Bracelet	bpp	1.20	1.14	1.16
	PSNR	47.27	46.13	45.70
Knight	bpp	1.12	1.049	1.036
	PSNR	45.50	44.78	44.56

Table 3: The variation in the resulting compression rate and quality varies with change in tree height is highlighted. The block threshold to 80 and the block size to 4 for all the datasets under consideration. As the tree height is increased the sparsity of the residual levels in the tree is increased. With the block threshold fixed the quantization errors increase and slight decrease in the resulting PSNR and bpp.

We implemented a CPU based single-threaded decoder and light field renderer to measure the average decoding times while generating new views using ray tracing. To compute a required pixel value, each of the channels (YCoCg26) values are decoded independently and the corresponding RGB pixel value is computed. The average decode times: (1) Y-Channel: 2 – 5 microseconds (2) Co-Channel: 1 – 2 microseconds (3) Cg-Channel: 1 – 2 microseconds. The average time per pixel required for computing a new view using ray-tracing is 15 – 20 microseconds.

5 CONCLUSIONS, LIMITATIONS, & FUTURE WORK

Conclusion: We present a new method (RLFC) for encoding LFI by constructing a hierarchy based on key views. Our method provides random access to the LF pixel values with one level of indirection and also supports parallel and progressive decompression. We have implemented our method on the two plane 4D parameterization of the light fields and highlight the performance. The average decompression time of block of pixels is approximately 2 – 5 microseconds and can be used for interactive application. As compared to prior random-access LFI compression methods, we observe 5 – 10× improvement in compression rates for similar PSNR quality. Our

approach is quite simple and general, and the implementation operations consist of memory reads, bit manipulation, and simple arithmetic operations.

Limitations: Our approach has some limitations. The reconstruction quality of our method for a sparsely sampled light fields can be low. Our algorithm uses filtering of spatially close LF samples to compute the representative key views. In a sparsely sampled light field, the nearby samples may not exhibit high level of spatial correlation. Moreover, our method doesn’t provide fine grained control over the reconstruction quality with respect to the encoding parameters. Therefore, a small change in the parameters can significantly degrade the quality. Even though RLFC offers improved compression rates over prior random-access methods, it is still lower than high-efficiency LFI compression schemes (10 – 20X lower).

Future Work: Our approach is general and can be applied to other light field parameterizations. Our compression and decompression algorithm involve simple memory and arithmetic operations and are a good candidate for hardware implementation. Our method can be extended to handle sparse light fields by replacing the filtering approach to construct the representative key views (Section 3.1) with a better method that takes sparse sampling into account.

REFERENCES

- Edward H Adelson, James R Bergen, et al. 1991. The plenoptic function and the elements of early vision. (1991).
- Thaddeus Beier and Shawn Neely. 1992. Feature-based image metamorphosis. In *ACM SIGGRAPH Computer Graphics*, Vol. 26. ACM, 35–42.
- Clemens Birkelbauer, Simon Opelt, and Oliver Bimber. 2013. Rendering gigaray light fields. In *Computer Graphics Forum*, Vol. 32. Wiley Online Library, 469–478.
- Chris Buehler, Michael Bosse, Leonard McMillan, Steven Gortler, and Michael Cohen. 2001. Unstructured lumigraph rendering. In *Proceedings of the 28th annual conference on Computer graphics and interactive techniques*. ACM, 425–432.
- Jin-Xiang Chai, Xin Tong, Shing-Chow Chan, and Heung-Yeung Shum. 2000. Plenoptic sampling. In *Proceedings of the 27th annual conference on Computer graphics and interactive techniques*. ACM Press/Addison-Wesley Publishing Co., 307–318.
- Shing-Chow Chan and Heung-Yeung Shum. 2000. A spectral analysis for light field rendering. In *Image Processing, 2000. Proceedings. 2000 International Conference on*, Vol. 2. IEEE, 25–28.
- Jie Chen, Junhui Hou, and Lap-Pui Chau. 2018. Light Field Compression With Disparity-Guided Sparse Coding Based on Structural Key Views. *IEEE Transactions on Image Processing* 27, 1 (2018), 314–324.
- Shenchang Eric Chen and Lance Williams. 1993. View interpolation for image synthesis. In *Proceedings of the 20th annual conference on Computer graphics and interactive techniques*. ACM, 279–288.
- Wei-Chao Chen, Jean-Yves Bouguet, Michael H. Chu, and Radek Grzeszczuk. 2002. Light Field Mapping: Efficient Representation and Hardware Rendering of Surface Light Fields. In *Proceedings of the 29th Annual Conference on Computer Graphics and Interactive Techniques (SIGGRAPH ’02)*. ACM, New York, NY, USA, 447–456. <https://doi.org/10.1145/566570.566601>
- Abe Davis, Marc Levoy, and Fredo Durand. 2012. Unstructured light fields. In *Computer Graphics Forum*, Vol. 31. Wiley Online Library, 305–314.
- T. Ebrahimi, S. Foessel, F. Pereira, and P. Schelkens. 2016. JPEG Pleno: Toward an Efficient Representation of Visual Reality. *IEEE MultiMedia* 23, 4 (Oct 2016), 14–20. <https://doi.org/10.1109/MMUL.2016.64>
- Bernd Girod, Chuo-Ling Chang, Prashant Ramanathan, and Xiaoqing Zhu. 2003. Light field compression using disparity-compensated lifting. In *Acoustics, Speech, and Signal Processing, 2003. Proceedings. (ICASSP ’03). 2003 IEEE International Conference on*, Vol. 4. IEEE, IV–760.
- Steven J. Gortler, Radek Grzeszczuk, Richard Szeliski, and Michael F. Cohen. 1996. The Lumigraph. In *Proceedings of the 23rd Annual Conference on Computer Graphics and Interactive Techniques (SIGGRAPH ’96)*. ACM, New York, NY, USA, 43–54. <https://doi.org/10.1145/237170.237200>
- Insung Ihm, Sanghoon Park, and Rae Kyoungh Lee. 1997. Rendering of spherical light fields. In *Computer Graphics and Applications, 1997. Proceedings., The Fifth Pacific Conference on*. IEEE, 59–68.
- Aaron Isaksen, Leonard McMillan, and Steven J Gortler. 2000. Dynamically reparameterized light fields. In *Proceedings of the 27th annual conference on Computer graphics and interactive techniques*. ACM Press/Addison-Wesley Publishing Co., 297–306.

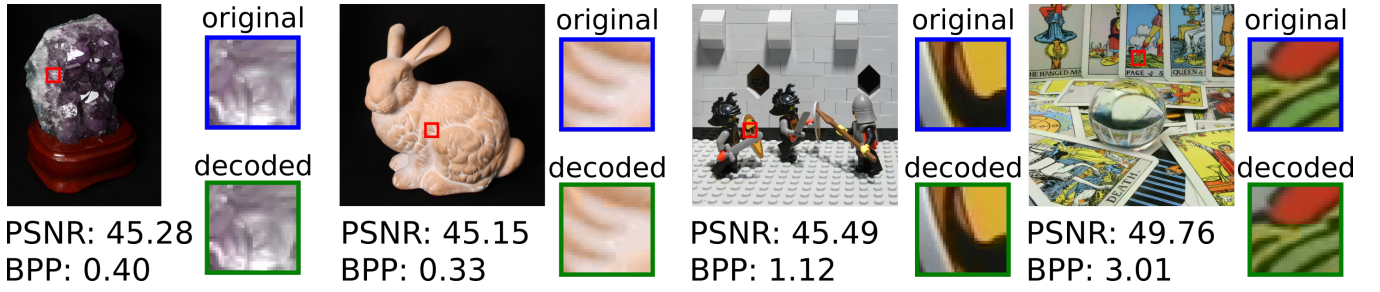


Figure 6: The zoomed in comparisons between original and decoded LF images from our method are shown. A 32×32 small regions highlighted in red boxes are scaled to 512×512 to compare the visual quality between original and compressed images. we observe no degradation in the visual quality in images compressed using our method.

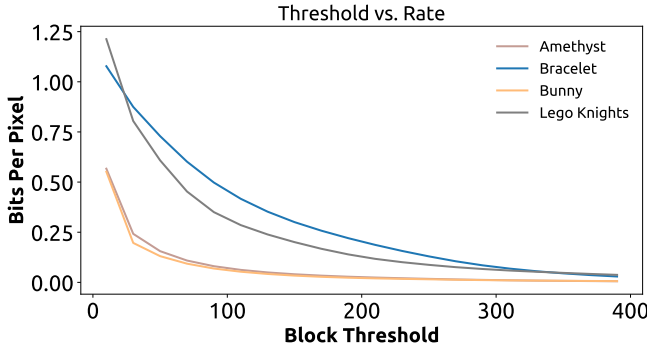


Figure 7: The variation of the compression rate (bpp) with change in the block threshold is plotted. The *tree height* to 3 and *block size* to 2 and vary the *block threshold*. With increase in the *block threshold* the quantization errors and the bpp decreases for all the LF datasets.

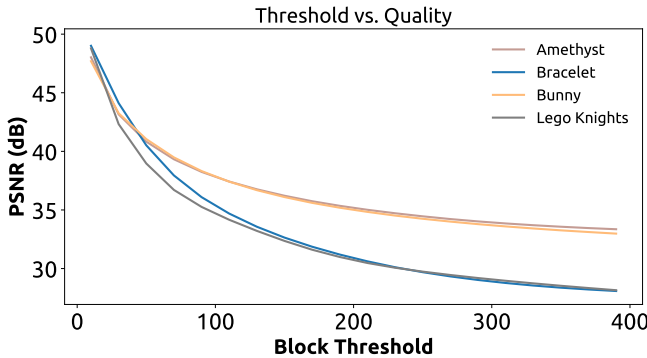


Figure 8: The variation of the decompression quality (PSNR) with change in the *block threshold* is plotted. The *tree height* to 3 and *block size* to 2 and vary the *block threshold*. With increase in the *block threshold* the quantization errors and the PSNR decreases for all the LF datasets.

A Jagmohan, A Sehgal, and N Ahuja. 2003. Compression of lightfield rendered images using coset codes. In *Signals, Systems and Computers, 2004. Conference Record of the Thirty-Seventh Asilomar Conference on*, Vol. 1. IEEE, 830–834.

Andrew Jones, Ian McDowall, Hideshi Yamada, Mark Bolas, and Paul Debevec. 2007. Rendering for an interactive 360 light field display. *ACM Transactions on Graphics (TOG)* 26, 3 (2007), 40.

Shinjini Kundu. 2012. Light field compression using homography and 2D warping. In *Acoustics, Speech and Signal Processing (ICASSP), 2012 IEEE International Conference on*. IEEE, 1349–1352.

Marc Levoy and Pat Hanrahan. 1996. Light Field Rendering. In *Proceedings of the 23rd Annual Conference on Computer Graphics and Interactive Techniques (SIGGRAPH*

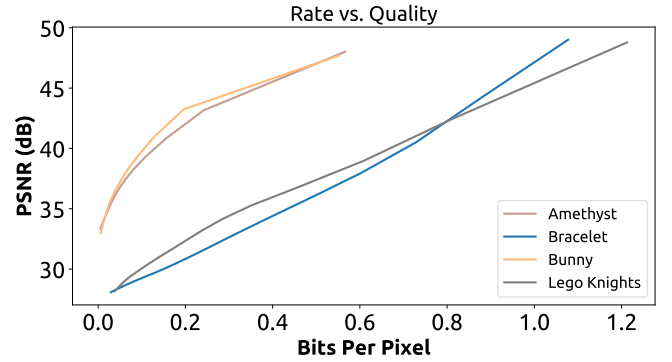


Figure 9: The variation of the decompression quality (PSNR) with change in compression rate (bpp) is highlighted. The *tree height* to 3 and *block size* to 2 and vary the *block threshold* and resulting bpp and PSNR values are plotted for the LF datasets.

'96). ACM, New York, NY, USA, 31–42. <https://doi.org/10.1145/237170.237199>

Zhouchen Lin and Heung-Yeung Shum. 2000. On the number of samples needed in light field rendering with constant-depth assumption. In *Computer Vision and Pattern Recognition, 2000. Proceedings. IEEE Conference on*, Vol. 1. IEEE, 588–595.

Andrew Lippman. 1980. Movie-maps: An application of the optical videodisc to computer graphics. In *Acm Siggraph Computer Graphics*, Vol. 14. ACM, 32–42.

Dong Liu, Lizhi Wang, Li Li, Zhiwei Xiong, Feng Wu, and Wenjun Zeng. 2016. Pseudo-sequence-based light field image compression. In *Multimedia & Expo Workshops (ICMEW), 2016 IEEE International Conference on*. IEEE, 1–4.

Marcus Magnor and Bernd Girod. 2000. Data compression for light-field rendering. *IEEE Transactions on Circuits and Systems for Video Technology* 10, 3 (2000), 338–343.

H. S. Malvar, G. J. Sullivan, and S. Srinivasan. 2008. Lifting-Based Reversible Color Transformations for Image Compression. In *SPIE Applications of Digital Image Processing*. International Society for Optical Engineering. <http://research.microsoft.com/apps/pubs/default.aspx?id=102040>

Leonard McMillan and Gary Bishop. 1995. Plenoptic modeling: An image-based rendering system. In *Proceedings of the 22nd annual conference on Computer graphics and interactive techniques*. ACM, 39–46.

Ren Ng, Marc Levoy, Mathieu Brédif, Gene Duval, Mark Horowitz, and Pat Hanrahan. 2005. Light field photography with a hand-held plenoptic camera. *Computer Science Technical Report CSTR 2*, 11 (2005), 1–11.

Jörn Nystad, Anders Lassen, Andy Pomianowski, Sean Ellis, and Tom Olson. 2012. Adaptive Scalable Texture Compression. In *Proceedings of the ACM SIGGRAPH/EUROGRAPHICS conference on High Performance Graphics (HPG '12)*. Eurographics Association, 105–114.

J-R Ohm, Gary J Sullivan, Heiko Schwarz, Thiw Keng Tan, and Thomas Wiegand. 2012. Comparison of the coding efficiency of video coding standards including high efficiency video coding (HEVC). *IEEE Transactions on circuits and systems for video technology* 22, 12 (2012), 1669–1684.

Cristian Peria and Pedro Assuncao. 2016. High efficiency coding of light field images based on tiling and pseudo-temporal data arrangement. In *Multimedia & Expo Workshops (ICMEW), 2016 IEEE International Conference on*. IEEE, 1–4.

Christian Perwass and Lennart Wietzke. 2012. Single lens 3D-camera with extended depth-of-field. In *Human Vision and Electronic Imaging XVII*, Vol. 8291. International Society for Optics and Photonics, 829108.

- Ingmar Peter and Wolfgang Straßer. 2001. The wavelet stream: Interactive multi resolution light field rendering. In *Rendering Techniques 2001*. Springer, 127–138.
- I. Viola, M. Aghajani, and T. Ebrahimi. 2017. Comparison and Evaluation of Light Field Image Coding Approaches. *IEEE Journal of Selected Topics in Signal Processing* 11, 7 (Oct 2017), 1092–1106. <https://doi.org/10.1109/JSTSP.2017.2740167>
- Bennett Wilburn, Neel Joshi, Vaibhav Vaish, Eino-Ville Talvala, Emilio Antunez, Adam Barth, Andrew Adams, Mark Horowitz, and Marc Levoy. 2005. High performance imaging using large camera arrays. In *ACM Transactions on Graphics (TOG)*, Vol. 24. ACM, 765–776.
- J. Yu. 2017. A Light-Field Journey to Virtual Reality. *IEEE MultiMedia* 24, 2 (Apr 2017), 104–112. <https://doi.org/10.1109/MMUL.2017.24>